Advances in the numerical modeling of sediment failure during the development of a continental margin

Eric W.H. Hutton *, James P.M. Syvitski

Environmental and Computation and Imaging Group, INSTAAR, University of Colorado at Boulder, 1560 30th Street, Campus Box 450, Boulder, CO 80309-0450, USA

Abstract

The *SedFlux* model is modified to more realistically simulate the distributions of seafloor geotechnical parameters during the growth of a seismically active continental margin. Alternative methods are provided for the prediction of the coefficient of consolidation, remolded shear strength, internal friction angle, sediment cohesion, dynamic viscosity and excess pore pressure. The new methods improve simulations of the architecture of basin deposits through the dynamics within the slope stability and debris flow modules. The new formulation shows sediment failures to be more frequent but smaller in size, and to occur at larger water depths. However, the overall architecture is not significantly different. *SedFlux* is then used to examine the role of global sea level fluctuations on the location and dimensions of sediment failure, and the subsequent transport of sediment to the deep ocean. More sediment failures are predicted to occur during periods of falling or low sea level conditions, and to be confined to the upper continental slope (500 ± 250 m water depth). The shallower failures are more characteristic of the period represented by the last two episodes of low sea level (i.e. during the Late Pleistocene), affected by the magnitude of the sea level fluctuation. Most of the predicted failures have thickness < 10 m. Larger failures occur during periods of rising or high sea level stand. © 2003 Elsevier B.V. All rights reserved.

Keywords: sediment failure; geotechnical modeling; sea level fluctuations; debris flow transport

1. Introduction

Advanced numerical models concerning the formation of sedimentary strata fuse information from the atmosphere, ocean and regional geology. These models apply a process response approach to how sediment transport processes form and destroy strata, and influence the developing architecture along continental margins. The *SedFlux* model is an example, able to simulate the lithologic character of basin stratigraphy by integrating a series of process-based event modules to:

● spread the fluvial bedload of coarser material across supratidal and subtidal portions of an evolving delta plain,

● disperse suspended sediment from a model river through either surface (hypopycnal: Syvitski et al., 1998) or subsurface (hyperpycnal: Skene et al., 1997) plumes,

* Corresponding author.
E-mail addresses: huttone@colorado.edu
(E.W.H. Hutton), syvitski@colorado.edu (J.P.M. Syvitski).

● disperse and sort seafloor sediment through ocean storm events (wave–current interactions, Wright et al., 2001; Harris and Wiberg, 2001), failures of margin deposits (Syvitski and Alcott, 1995; Syvitski and Hutton, 2003) and the subsequent transport of material as turbidity currents (Mulder et al., 1997; Pratson et al., 2001) or debris flows (Pratson et al., 2000; Imran et al., 2001), and

● change the accommodation due to subsidence, tectonics (Steckler, 1999; Syvitski and Hutton, 2001), and compaction of the final deposit (Bahr et al., 2001).

SedFlux processes and deposits interact with the ever-evolving boundary conditions (seafloor bathymetry, sea level, and coastline position) to create a sedimentary architecture (Skene et al., 1998). The primary parameters modeled by *SedFlux* in the time and space domain are grain size, bulk density, porosity, and permeability.

This paper highlights recent modifications to two-dimensional (2D) *SedFlux* with particular reference to the analysis of the geotechnical properties of the evolving deposits. For a complete explanation of the components of *SedFlux* that this paper does not address, we refer the reader to Syvitski and Hutton (2001). In prior versions of the model (i.e. O'Grady and Syvitski, 2001), the geotechnical parameters (coefficient of consolidation, remolded strength, internal friction angle, sediment cohesion, sediment dynamic viscosity) were held constant for the entire model run (i.e. in the time–space domain). By allowing these parameters to vary in time and space depending on local conditions, the dynamics of sediment failure and debris flow transport are influenced in the new model. The paper examines the consequences of these model changes. Finally the growth of a seismically active continental margin is simulated to examine the role of sea level fluctuations on the location and dimensions of sediment failure, and the subsequent transport of sediment to the deep ocean. While scientists have argued for the strong influence of sea level position on sediment failure (e.g. May et al., 1983; Mitchum et al., 1977; Ross et al., 1994), others have suggested a more limited influence of sea level on sediment failure (Farre et al., 1983).

2. Theory

The failure of continental margin sediment and its subsequent movement plays an important role in the transferring sediment into deeper water. The *SedFlux* method for determining sediment failure is based on the following pathway:

● construct possible elliptical failure planes at specified time intervals (Syvitski and Hutton, 2001),

● calculate the local slope between columns of cells along failure planes,

● calculate excess pore pressure in the model domain,

● calculate load at each cell above potential failure plane (weight of sediment minus the excess pore pressure),

● calculate the sediment internal friction angle based on soil properties,

● calculate the sediment cohesion of the local deposit,

● determine earthquake load (horizontal and vertical acceleration),

● calculate Janbu factor of safety of each potential failure plane,

● calculate the failure volume, and

● determine properties of the failed material (en masse) and decide whether material moves as a debris flow or turbidity current.

Below we provide a description of the new algorithms employed in 2D *SedFlux* for determining these geotechnical parameters at the local scale.

2.1. Excess pore pressure

2D *SedFlux* can employ one of three methods for the calculation of excess pore pressure. The Gibson (1958) Method is simple but elegant. It assumes that excess pore pressures are generated as a function of the rate at which sediment is added to a sediment column and the average grain size of the material (homogenized) in the sediment column. It is used in Global Model set up described below. The Exponential Method (Bardet, 1997) is more numerically taxing as it tracks pore pressures in each sediment layer (cell) within a sediment column, given informa-

tion on the overlying load and average grain size comprising each sedimentary layer. It assumes that excess pore pressure falls off exponentially with sediment load, but uniquely within each cell. The Kozeny–Carman excess pore pressure method is an advanced one-dimensional (1D) solution to sediment consolidation and the material properties of each cell within a sediment column.

2.1.1. Gibson Method

The excess pore pressure, u_i, can be obtained from consolidation theory under the assumption that excess pressures are entirely the result of trapping pore water in compacting, fine-grained sediment of low permeability. Gibson's graphical approximation (1958) is then (after Syvitski and Alcott, 1995):

$$u = \frac{\gamma' z}{6.4 \left(1 - \frac{T}{16}\right)^{17} + 1} \tag{1}$$

where γ' is the submerged specific weight of the sediment, z is depth of the failure plane with re-

spect to the seafloor, and T is a constant defined as

$$T \equiv \frac{m^2 t}{C_v} \tag{2}$$

and m is sedimentation rate, t is time of deposition, C_v is the consolidation coefficient for the sediment (also known as hydraulic conductivity), and is a function of grain size such that for sands $C_v \approx 10^{-7}$ m^2/s and for clay $C_v \approx 10^{-9}$ m^2/s (Loseth, 1999; Freeze and Cherry, 1979, p. 29).

2.1.2. Exponential Method

Following the logic of Bardet (1997, p. 312), then:

$$u_i = \sigma(1 - U) \tag{3}$$

where σ is the load of the overlying sediment, and U is the degree of consolidation, and (Bardet, 1997, p. 312):

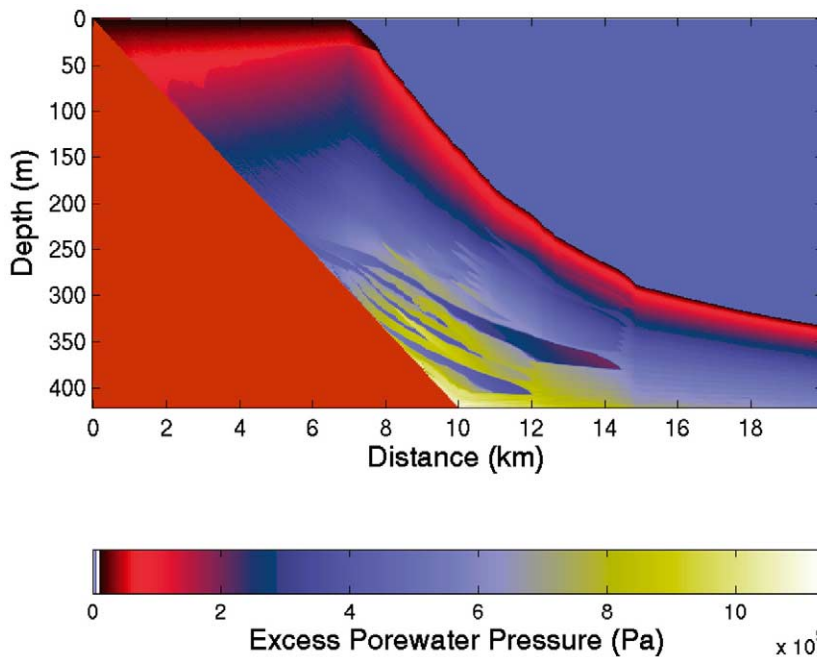$$U = \frac{1}{H} \int_0^H U_y \, dy \tag{4}$$

Fig. 1. Simulation of an idealized basin using *SedFlux*. Excess pore pressure is calculated with the Exponential Method (Eqs. 3–6). Debris flows within the stratigraphic column and located near the base of the slope are coarser (and therefore have reduced excess pore pressures) than the surrounding very fine-grained hemipelagic sediments.

$$U(T_v) = \begin{cases} \sqrt{\dfrac{4}{\pi}T_v} & \text{for } T_v < 0.2827 \\ 1 - \dfrac{8}{\pi^2}\exp\left(-\dfrac{\pi^2}{4}T_v\right) & \text{for } T_v \geq 0.2827 \end{cases} \quad (5)$$

T_v is the dimensionless time factor:

$$T_v = \frac{C_v t}{H^2} \quad (6)$$

and H is the thickness of the drainage layer (the sediment package in a *SedFlux* simulation). Fig. 1 provides an example of a 2D *SedFlux* simulation of an idealized basin demonstrating the Exponential Method (Eqs. 3–6) pertaining to the calculation of excess pore pressure. River sediment was added to the basin using daily time steps over 10 000 yr. Debris flows within the stratigraphic column and located near the base of the slope are coarser than the surrounding very fine-grained hemipelagic sediments that have accumulated from shelf bottom boundary layer and river plume transport. The result is that the debris flows are able to dewater faster (and therefore have reduced excess pore pressures) than the surrounding hemipelagic muds.

2.1.3. Kozeny–Carman Method

Following consolidation theory (Furbish, 1997, p. 335), then:

$$\rho_w g \varphi \frac{\partial u_i}{\partial t} - \varphi \frac{\partial \sigma}{\partial t} = \frac{\partial}{\partial z} k \frac{\partial u}{\partial z} \quad (7)$$

where ρ_w is the fluid density, g is acceleration due to gravity, φ is a coefficient for sediment compressibility, k is permeability (m/s) using the Kozeny–Carman Formula (Bardet, 1997, p. 182):

$$k = \frac{\gamma_w}{5f\mu_w S^2}\frac{e^3}{1+e} \quad (8)$$

where S is specific surface area $S = (6/\sqrt{D_{max}D_{min}})$ (D_{max} and D_{min} are the maximum and minimum grain diameters, respectively), f is shape factor where $f = 1.1$ for rounded grains, 1.25 for subrounded grains and 1.4 for angular grains, μ_w is the dynamic viscosity of water, γ_w is the unit weight of water, and e is void ratio.

2.2. Sediment internal friction angle

2.2.1. Friction angle as a function of grain size

The internal friction angle ϕ (°) can vary with grain size, D:

$$\phi = \begin{cases} 25°, & D > 2 \text{ mm} \\ 27°, & 0.6 < D \leq 2 \text{ mm} \\ 32°, & 0.2 < D \leq 0.6 \text{ mm} \\ 36°, & D < 0.2 \text{ mm} \end{cases} \quad (9)$$

and can be further modified by the relative density ρ_r using

$$\phi = \begin{cases} \phi - 1°, & \rho_r < 0.5 \\ \phi + 4°, & \rho_r > 0.75 \end{cases} \quad (10)$$

where the relative density is defined as

$$\rho_r = \frac{e_{max} - e}{e_{max} - e_{min}} \quad (11)$$

where e is void ratio within the sediment column, e_{max} is the maximum void ratio of the sediment, and e_{min} is the void ratio of the sediment in its closest pack condition ($e = 0.3$).

2.2.2. Friction angle as a function of sediment load

Based on lab experiments on London Clay by Bishop (1966) (also Bardet, 1997, p. 368), the following empirical relationship can be used to estimate the internal friction angle:

$$\tan \phi = A p \sigma_e^{p-1} \quad (12)$$

where A and p are empirical constants with $p = 0.6$, $A = 0.69$, and σ_e is the effective stress or effective load (in MPa).

2.3. Sediment cohesion

The cohesion value c for muddy sediment is modeled as a function of effective load (Bardet, 1997; p. 368):

$$c = A(1-p)\sigma_e^p \quad (13)$$

where parameters are defined as in Eq. 12 and Bishop (1966). For sandy material $c = 0$.

2.4. Earthquake loading

During an earthquake, a seismic wave exerts an

additional body force on a deposit. Therefore, an earthquake probability frequency distribution (i.e. earthquake intensity as measured at the slip plane versus return interval) is used to explore dynamic slope stability. For such a scenario, associated ground acceleration a_e is acquired for each stability analysis performed in a simulation (typical values of mean a_e range from 0 to 0.15 times gravity). Earthquake accelerations are generated as a distribution around user-specified mean acceleration as shown in (Fig. 2).

The vertical weight, W_v, of a sediment column is then modified by the earthquake load, such that:

$$W_v = M(g + a_v) \tag{14}$$

where M is the mass of sediment column, g is the acceleration due to gravity, a_v is the vertical acceleration due to the earthquake. The horizontal pull (or, weight) on a sediment column is simply:

$$W_h = Ma_h \tag{15}$$

where a_h is the horizontal acceleration due to the earthquake. Typically a_h is set to be 10% of a_v in the *SedFlux* experiments discussed below.

2.5. Factor of safety analysis

Because *SedFlux* is designed to simulate the fill of sedimentary basins having complex bathymetric shapes, a finite slope stability routine is considered most appropriate. The geometry and location of failures are determined using the Janbu factor of safety analysis with the method of slices (Janbu, 1968; Anderson and Richards, 1987). The Janbu method is useful for the analysis of noncircular slip surfaces. The method ignores interslice forces, although a technique is available to correct for these forces (Anderson and Richards, 1987). Interslice forces are invariably small, adjusting the calculated factor of safety by less than 10%, depending on the geometry of the problem as well as the soil condition. *SedFlux* examines a series of possible elliptical failure surfaces for stability. A failure surface is found by connecting one point of the seafloor to another with a quarter ellipse. *SedFlux* examines all such failure planes within a profile. The failure package is divided into N vertical slices and the stability of the possible failure plane is characterized through its factor of safety as:
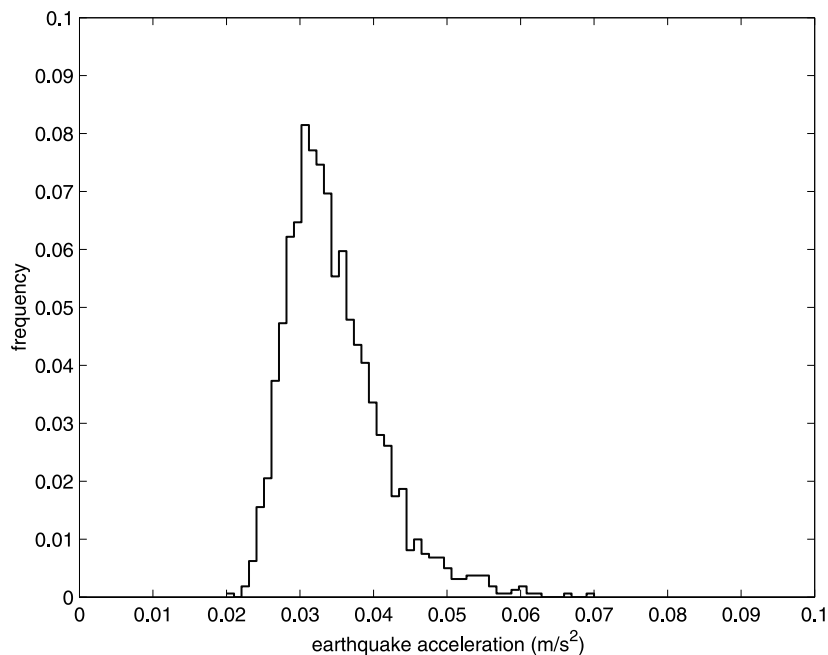

Fig. 2. The probability density function of earthquake accelerations around a specified mean of 0.035 m/s², generated and used by *SedFlux* for the simulation of a continental margin shown in Fig. 4.

$$F_\text{T} = \frac{\sum_{i=0}^{N-1} \left[b_i \left(c_i + \left(\frac{W_{\text{v}_i}}{b_i} - u_i \right) \tan \phi_i \right) \frac{\sec \alpha_i}{1 + \frac{\tan \alpha_i \tan \phi_i}{F_\text{T}}} \right]}{\sum_{i=0}^{N-1} W_{\text{v}_i} \sin \alpha_i + \sum_{i=0}^{N-1} W_{\text{h}_i} \cos \alpha_i} \quad (16)$$

where the subscript i denotes a vertical slice, F_T is the factor of safety for the entire sediment volume (with iterative convergence to a solution), b is the width of the slice (or sediment column), c is sediment cohesion (see Eq. 13); f is internal friction angle (see Eq. 9 or Eq. 12), W_v is vertical weight of the column (see Eq. 14), α is the slope of failure plane, W_h is horizontal pull on column (see Eq. 15), and u is excess pore pressure (see Eq. 1, Eq. 3 or Eq. 7). Wilson and Keefer (1983) provide another comparable method of introducing ground accelerations to a factor of safety analysis. Neither method however includes the contribution of water pressures generated by the earthquake itself, although in principle *SedFlux* could also be configured to include that phenomenon.

If the static factor of safety is found to be less than some threshold (for this study, we used a value of 1.0), then the sediment is failed and moved downslope as a sediment gravity flow, otherwise it is deemed to be stable. The Janbu method neglects the influence of fractures, although in principle *SedFlux* could be configured to include that phenomenon.

2.6. Debris flow dynamics

Debris flows are modeled after the properties of a Bingham plastic (viscoplastic) fluid, with deformation driven by the excess of stress beyond the yield stress (Pratson et al., 2000; Imran et al., 2001). The model neglects the tangential stress acting on the water–mud interface, because the viscosity of water is much smaller than that of the mud, and the basal shear of the mud flow is much greater than the interfacial shear (Syvitski and Hutton, 2003). In addition, there is a no slip condition on the slide bottom. Syvitski and Hutton (2003) give the details of the governing equations. The main thing to note is that the debris flow dynamics depend on (among other things)

the shear strength (τ_y) and dynamic viscosity (μ) of the debris flow. *SedFlux* now calculates both of these parameters based on local conditions. The shear strength here is that of the already moving debris flow, and so we calculate a remolded shear strength that is based on the shear strength of the sediment before it is moved.

2.7. Remolded shear strength

The remolded shear strength τ_r is calculated by one of three methods. In the *Plasticity Method* (Bardet, 1997, p. 393), the remolded strength is defined as a function of a soil plasticity index PI, such that:

$$\tau_\text{r} = \frac{(0.11 + 0.0037\text{PI})\sigma_\text{e}}{S_\text{t}} \quad (17)$$

where PI is a function of grain size ranging from 0.1 for sand to 0.5 for clay, and σ_e is the effective stress or effective load, S_t is the sediment sensitivity parameter used to convert sediment strength to remolded strength ($S_\text{t} \approx 5$, H.J. Lee, personal communication, 2001). The *Load Method* (Bardet, 1997, p. 368) defines τ_r as a power function of sediment load:

$$\tau_\text{r} = \frac{A\sigma_\text{e}^p}{S_\text{t}} \quad (18)$$

where A and m are coefficients (see Eq. 12 or Bishop, 1966). The *Grain size-Dependent Method* (Julien, 1995, p. 190) is defined as:

$$\tau_\text{r} = 0.1e^{\beta(C-0.05)} \quad (19)$$

where τ_y here is given in units of Pa, $\beta = 3, 13, 23$ for sand, silt and clay respectively, and C is the volume concentration where $C = 1-n$, with n (porosity) defined as:

$$n = \frac{\rho_\text{s} - \rho_\text{b}}{\rho_\text{s} - \rho_\text{w}} \quad (20)$$

where ρ_s is grain density, ρ_b is bulk sediment density, and ρ_w is pore water density.

2.8. Dynamic viscosity

The dynamic viscosity routine used in the *SedFlux* debris flow model is from Julien (1995):

$$\mu = \mu_w(1 + 2.5C + \exp(\vartheta(C - 0.05))) \qquad (21)$$

where μ_w is the dynamic viscosity of water, and the coefficient ϑ varies between 10 and 23, for sands through muds, respectively.

3. Numerical experimentation

3.1. Impact of local versus global geotechnical parameters

Five geotechnical parameters (coefficient of consolidation, remolded strength, internal friction angle, sediment cohesion, sediment dynamic vis-

cosity) are either held constant for the entire model run in the time–space domain (Global Model), or are allowed to vary and therefore more accurately reflect local conditions of the various sedimentary environments (Local Model). Two case histories are simulated: (1) the fill of a small and deep (30 km by 400 m) coastal (fjord) basin (Fig. 3A, B), and (2) the progradation of a 500 km by 1000 m deep continental margin (Fig. 3C, D). The coastal basin essentially has no shelf transport, sea level is held constant. Sediment supply varies around a mean yield. The model run duration is 10 000 yr and the architecture changes are recorded at daily time steps. The continental margin simulation covers a 200 000 yr
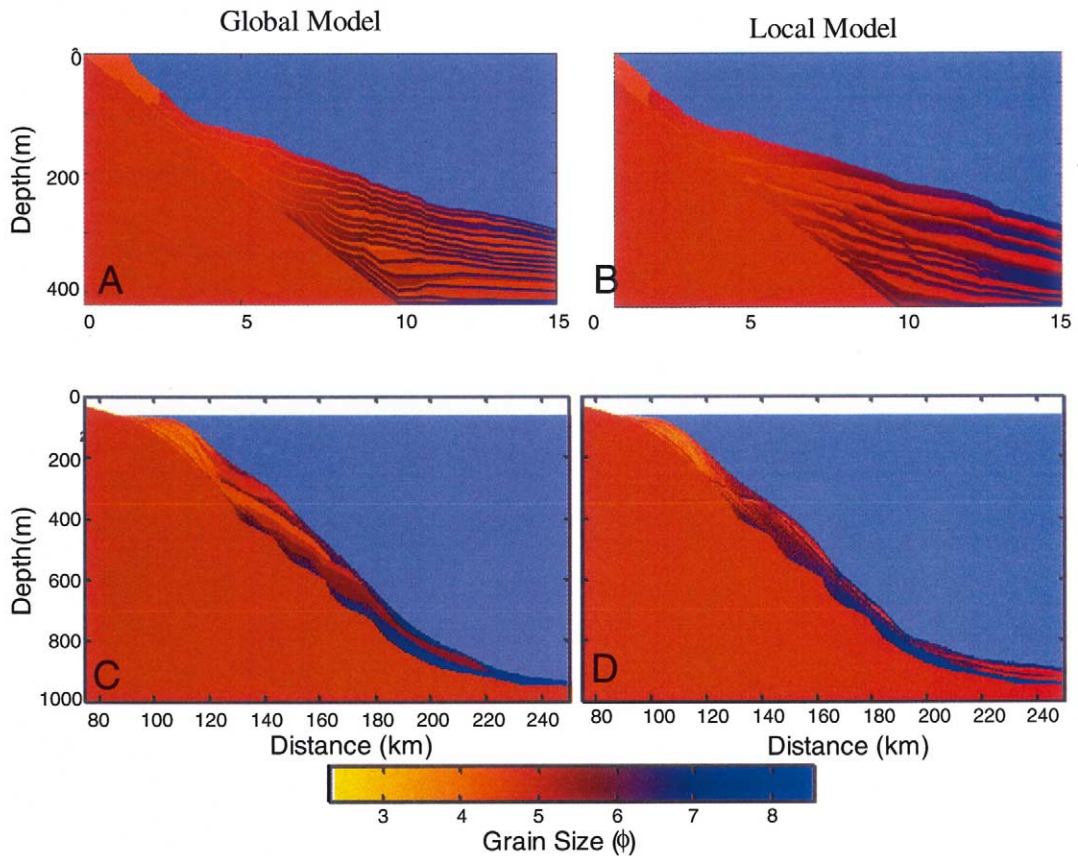

Fig. 3. *SedFlux* simulations of the sedimentary architecture of an idealized continental margin. Grain size is displayed in phi units in the depth and distance domain. (A) and (C) are simulations where key geotechnical parameters are held constant for the entire model run (i.e. in the time–space domain). (B) and (D) are simulations where the geotechnical parameters are allowed to vary in the time–space domain, and reflect the local sedimentary environment. Simulations (A) and (B) are for the 10 kyr fill of a small coastal basin. Simulations (C) and (D) are for the growth of a continental margin over a 200 kyr period (see Fig. 6 for full run).
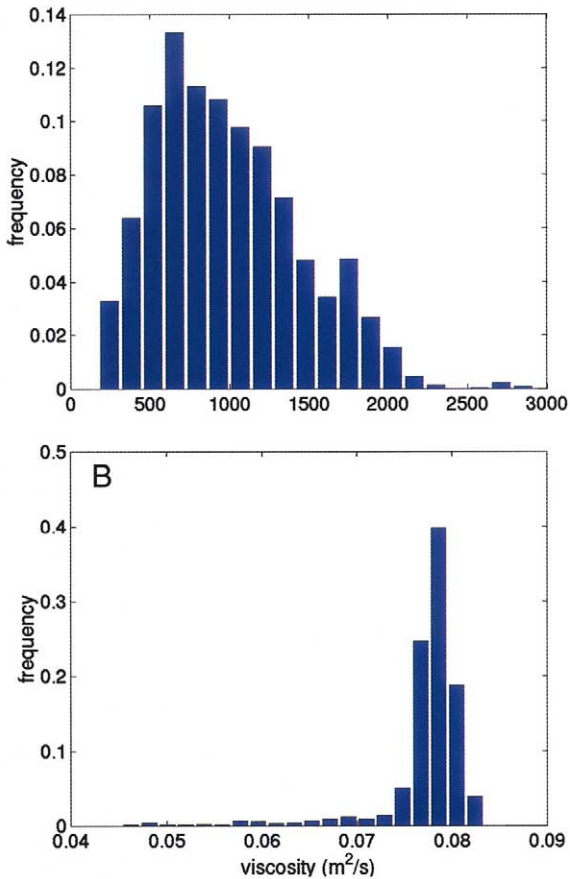
Fig. 4. The frequency distribution of geotechnical parameters predicted by 2D *SedFlux* and based on local sediment properties. The information is used in the debris flow module. (A) Remolded shear strength (Pa) using the Plasticity Method (Eq. 17). (B) Debris flow viscosity (m^2/s) using Eq. 21. Distributions can be compared with the constant domain values of 1 kPa and 0.08 m^2/s, respectively used in the Global Model.

period using 500 yr time steps. Shelf sediment transport is active, and sea level varies according to the 1–0.8 Myr global sea level curve. Sediment supply varies around a mean yield.

Unlike the Global Model, the Local Model will produce a frequency distribution of the geotechnical parameters used in the sediment failure module (Eq. 16) or the debris flow module (Eqs. 17–19). These distributions are not stochastically generated, but rather reflect the developing properties of local seafloor during the simulation. If,

for example, the *SedFlux* debris flow module uses domain constants for remolded strength and dynamic viscosity, then the behavior of modeled debris flows will simply reflect the bathymetry found seaward of the failure location (Figs. 3A, C). In contrast, if the Local Model is employed, with the remolded strength predicted for example by the Plasticity Method (Eq. 20), then the distribution of strength values used in the coastal basin simulation (Fig. 3B) ranges from 200 to 3000 Pa. Similarly, the distribution of dynamic viscosity values (Eq. 21), in the coastal basin simulation, ranges from 0.045 to 0.083 m^2/s (Fig. 4B). Similar variability in the local geotechnical parameters (coefficient of consolidation, internal friction angle, sediment cohesion, excess pore pressure) affects the location and size of sediment failures (Fig. 5).

One of the largest consequences of changing 2D *SedFlux* from a Global to Local Model is on the distribution of excess pore pressures, where the former is dependent on the rate of sediment accumulation, and the later is strongly influenced by the grain size and thus the hydraulic conductivity of the deposit. Examining Fig. 5A we note that the Global Model sees the highest number of failures in the shallow waters of the fjord where the sedimentation rates are highest. Failure frequency subsequently decreases seaward. The Gibson Method of defining excess pore pressures (Eq. 1) has no dependency on grain size and thus does not take into account the coarse particle size associated with the high rates of sediment accumulation, and their ability to quickly dewater. The Local Model uses the Plasticity Method (Eq. 3) that takes into account both grain size and accumulation rate. Thus failures occur more often in deeper water (160 m), with the number of failures decreasing both landward and seaward (Fig. 5B). The Local Model generates many more small (thin-skinned) failures, when compared to the Global Model (Fig. 5C, D).

These differences between Local and Global Methods lead to some differences in the final architecture of the deposits (Fig. 3). The general distribution of deposit thickness is very similar between the two approaches (Fig. 3), suggesting that initial boundary conditions dominate at the gross scale. However, the internal architecture is
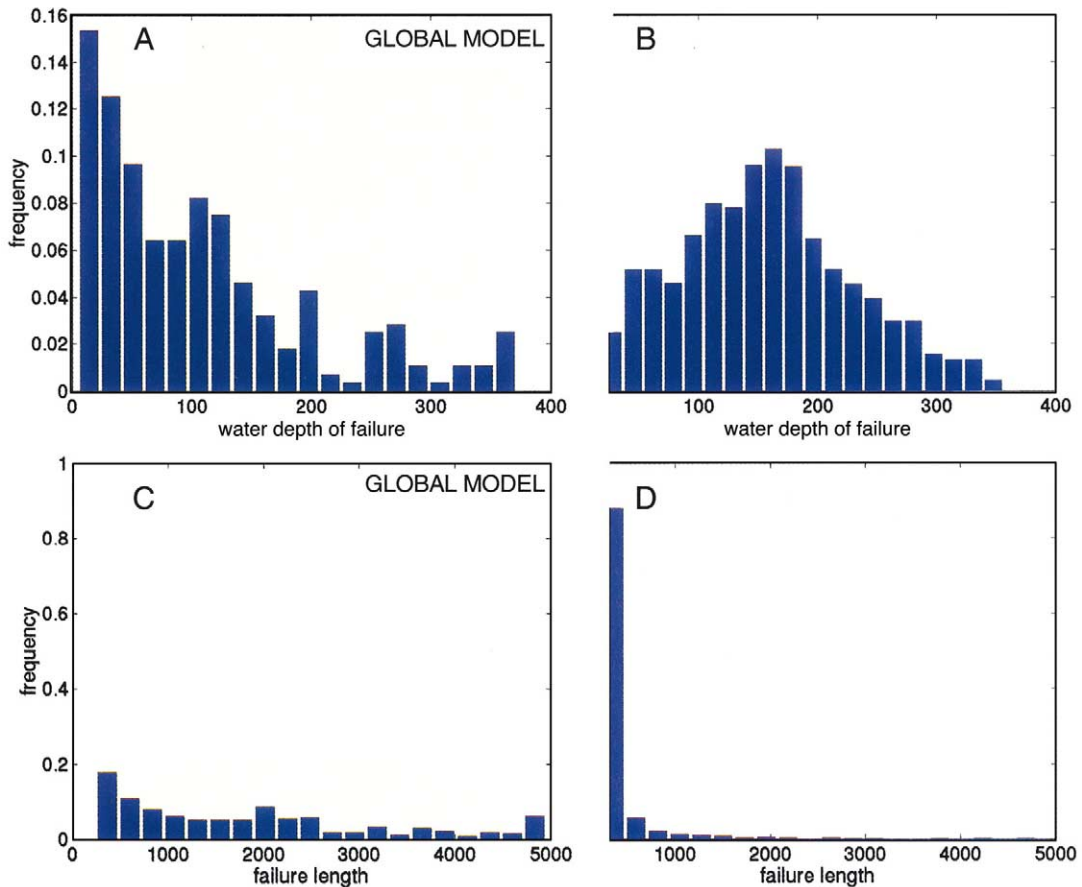
Fig. 5. Comparison of failure location (water depth) and failure size (length) generated by the Global Model, where key geotechnical parameters are held constant through the model simulation (see Fig. 3A), and the Local Model where these parameters vary according to local sedimentary properties (Fig. 3B). The modeled basin is after a small but deep fjord that essentially has no shelf sediment transport. Sea level is held constant during the model run, as is sediment supply.

very different. When applying the Local Model to the fjord environment, some of the simulated debris flow deposits appear graded (Fig. 3B). This is a consequence of the Local Model generating retrogressive failures where secondary and subsequent failures occur in shallower water associated with coarser grain size. The final amalgamated deposits appear graded in a coarsening upward manner, but not as a consequence of flow dynamics, rather from feedbacks within the failure dynamics. Using the continental margin test basin (Fig. 3C, D), the Global Model produces a few thick debris flows that deposit along the continental margin. In contrast the Local Model produces a few thick debris flows that travel to the basin

floor, and many smaller debris flows that are retained on the continental slope.

3.2. Influence of sea level on the local model

The above experimentation is designed to show the impact of using the dynamics of the Local Model in 2D *SedFlux*. To examine the consequences, we apply the Local Model to the 1 Myr development of a seismically active (see Fig. 1) continental margin (500 km by 1000 m: Fig. 6). While the time step of each *SedFlux* module is at the dynamics of the subroutine (and varies from < 1 s for debris flow dynamics to 1 day for river plumes), the model architecture is
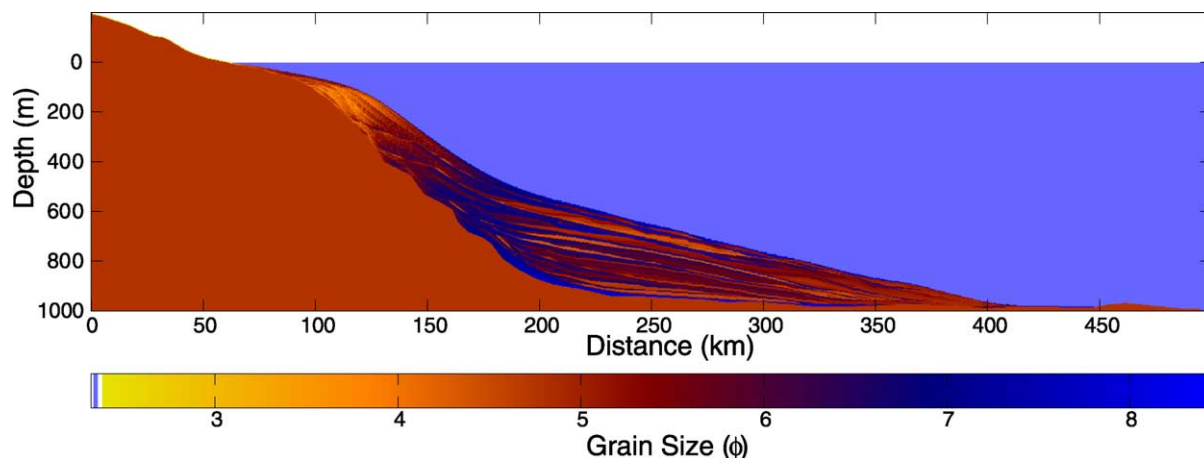
Fig. 6. A 1 Myr *SedFlux* simulation of an idealized and seismically active continental margin. The vertical resolution displayed is 3 m and the horizontal resolution is 300 m. See text for further details on the model's input and boundary conditions.

tracked in time steps of 500 yr. Sea level varies according to the global sea level curve (Fig. 7), based on the δO^{18} fractionation signal recovered from deep sea foraminifers. Sediment supply varies around a mean yield. It is known that climate will vary with sea level fluctuations (Warrick, 1993) and cause changes in the flux of sediment to the margin (see Morehead et al., 2001). We do not account for climate-influenced sediment delivery to further simplify our interpretation of the results. However *SedFlux* does simulate the transport of higher sediment loads when
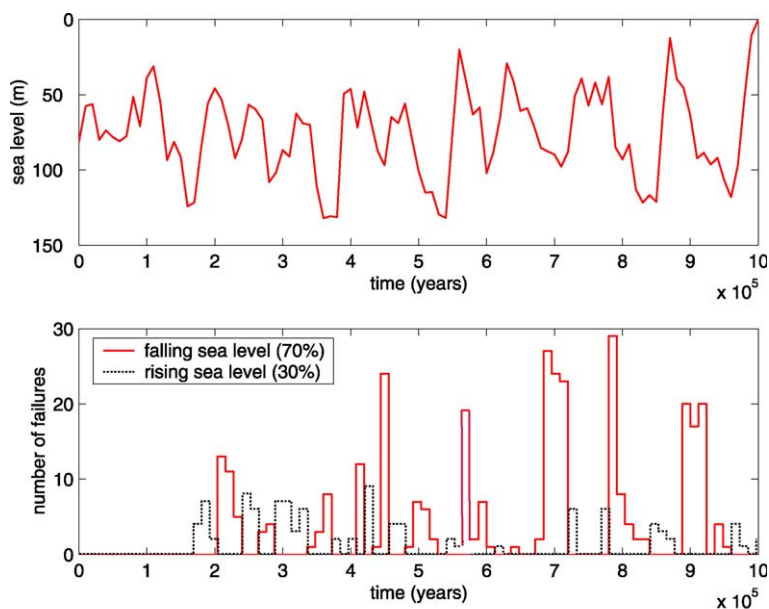

Fig. 7. Top panel: Global sea level curve of the last 1 Myr, based on the δO^{18} fractionation signal recovered from deep sea foraminifera (time = present at 10^6 yr). Bottom panel: Number of failures generated by *SedFlux* (see Fig. 6) with the modulating influence of sea level fluctuations. The first 200 kyr show few failures and reflect model spin up effects. Falling sea level conditions show comparatively more sediment failures than rising sea level.
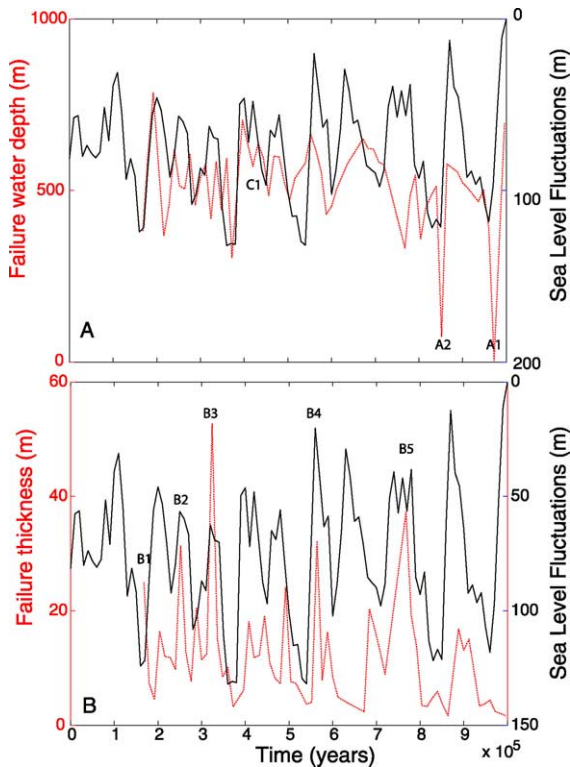
Fig. 8. Failure history of the *SedFlux* simulation shown in Fig. 6. Top panel: Most failures are located on the upper continental slope in 500 ± 250 m water depth. Between 500 and 600 kyr BP (C1) there is a high level of coherency between failure depth and sea level. The shallowest failures occurred during the previous two episodes of low sea level stand (A1 and A2). Bottom panel: Most of the failures have thickness < 10 m. The thickest failures occur during periods of rising or high sea level stand (located as B1–B5).

sea level stand (Fig. 7). Failures can occur at any sea level position depending on the prior depositional history. However during periods of falling or low sea level conditions, many more sediment failures can occur (by a factor of 3–5) than during comparable periods of rising or high sea level stand (Fig. 7). More failures occur in the most recent 0.5 Myr interval when sea level fluctuations are largest (Fig. 7). Except for the spin up period, there are very few 12 kyr intervals that have no failures registered.

Most of the model failures are located on the upper continental slope in 500 ± 250 m water depth (Fig. 8A, with details seen in Fig. 9A). Between 500 and 600 kyr BP (see C1 of Fig. 8A) there is a high level of coherency between the water depth of the sediment failure and position of the sea level. At other periods there is no coherency demonstrated. The shallowest failures occurred during the last two episodes of low sea level stand (identified as A1 and A2 on Fig. 8A).

Most failures have thickness < 10 m, although some can exceed 30 m (Fig. 8B, with details seen in Fig. 9B). The average thickness of sediment failure increases markedly during periods of rising or high sea level stand (identified as B1–B5 on Fig. 8B). No relationship exists between earthquake accelerations and the location of the sediment failures (Fig. 9A), nor between earthquake accelerations and the average thickness of the sediment failure (Fig. 9B).

4. Summary

The modular *SedFlux* model continues to develop and grow in sophistication. The new advances outlined above, demonstrate the impact of allowing key geotechnical parameters (coefficient of consolidation, remolded strength, internal friction angle, sediment cohesion, sediment dynamic viscosity) to vary in time and space depending on local conditions. Additionally, advanced routines for excess pore pressure vastly improve the location and dimensions of sediment failures. Together these changes to the dynamics of sediment failure and debris flow runout provide strong feedback to the geometry and architecture of the

sea level falls through the terrestrial erosion of exposed marine deposits. As a final simplification we have not employed the isostasy module in 2D *SedFlux* (readers are referred to O'Grady and Syvitski, 2001 who specifically examine the influence of isostasy). The resulting simulated architecture is a large fan built seaward of the initial bedrock bathymetry (Fig. 6) along with moderate (40 km) progradation of the shelf slope break. The first 200 kyr show few failures and this in part relates to model spin up effects (Fig. 7).

Sediment failures are lumped into 83 time intervals of 12 kyr each, for ease of comparison to the sea level curve. Results indicate that the number of sediment failures is highly influenced by the
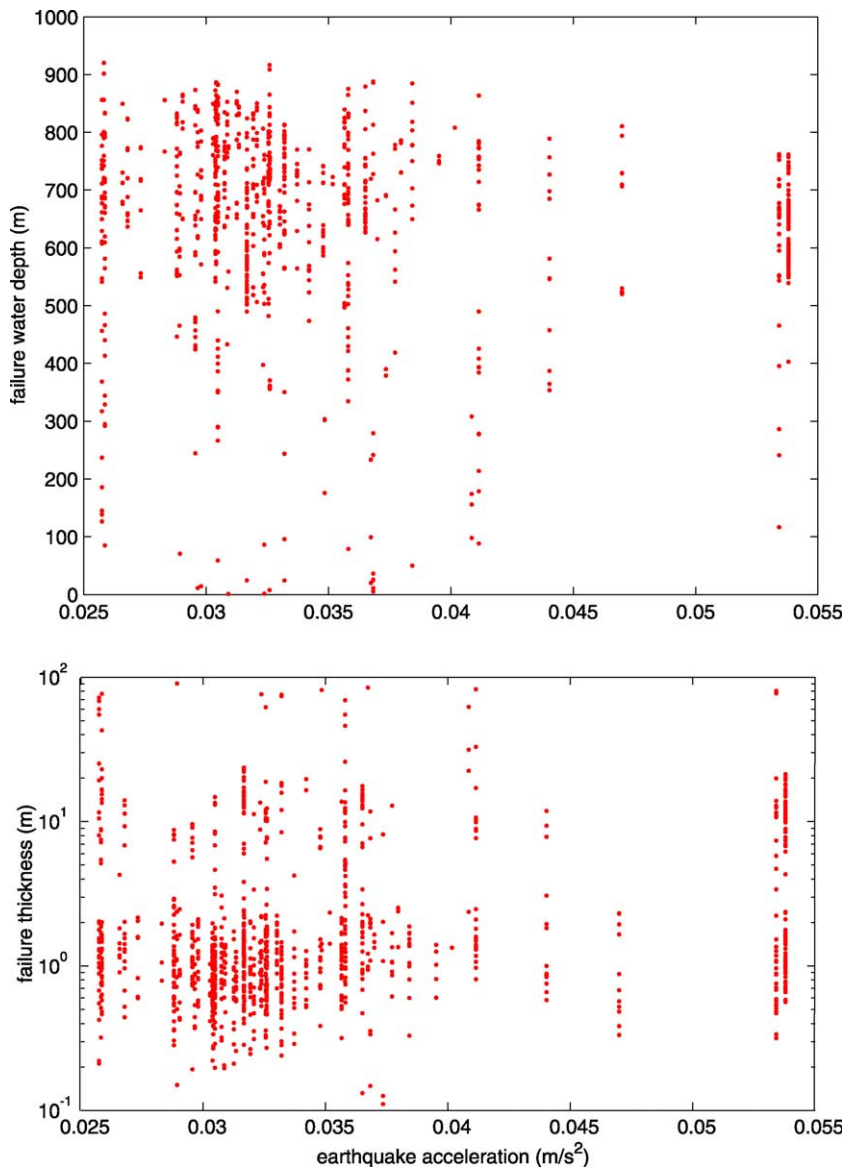
Fig. 9. The relationship between earthquake accelerations and the average water depth (m) of the sediment failure (top panel) and the average thickness of the sediment failure (bottom panel).

simulated basin stratigraphy. By producing more realistic frequency distributions of the geotechnical parameters that reflect the developing properties of local seafloor during the simulation, important feedbacks between sediment properties and processes are honored. For example, by allowing the *SedFlux* debris flow module to use predicted remolded strengths and viscosities, the

dynamics of debris flows reflect both the physical properties of the failed sedimentary mass as well as the bathymetry found seaward of the failure location.

The Exponential Method is much superior to the Gibson Method (as is the Kozeny–Carman Method) in the prediction of excess pore pressure, within the model domain. As a consequence sedi-

ment failures are predicted to be thinner and located in deeper water.

The final geometry of the modeled offshore sedimentary unit does not differ greatly when comparing simulations with Global or Local characterization of the sediment deposits. This likely shows the strong influence of initial boundary conditions, such as rate of sediment supply, sea level history, and initial bathymetry. However the internal architecture of the deposits can differ greatly when comparing the two methods (Fig. 3).

Retrogressive failures generated with the Local characterization method, can result from secondary failures occurring in progressively shallower water where sediment grain size is often coarser. The final amalgamated deposit appears to coarsen upward as a consequence of failure dynamics rather than flow dynamics.

The new Local Model demonstrates that the number of sediment failures is highly influenced by the sea level stand. More sediment failures occur during periods of falling or low sea level conditions, located on the upper continental slope in 500 ± 250 m water depth. The shallowest failures are predicted to have occurred during the last two episodes of low sea level stand, affected by the magnitude of their sea level amplitude. Most of the predicted failures have thickness < 10 m, with failure volume increasing markedly during periods of rising or high sea level stand.

Acknowledgements

References

Anderson, M.G., Richards, K.S., 1987. Slope Stability: Geotechnical Engineering and Geomorphology. Wiley, New York.

Bahr, D.B., Hutton, E.W.H., Syvitski, J.P., Pratson, L., 2001. Exponential approximation to compacted sediment porosity profiles. Comput. Geosci. 27, 691–700.

Bardet, J.P., 1997. Experimental Soil Mechanics. Prentice Hall, Upper Saddle River, NJ, 583 pp.

Bishop, A.W., 1966. The strength of soils as engineering materials. Géotechnique 36, 65–78.

Farre, J.A., McGregor, B.A., Ryan, W.B.F., Robb, J.M., 1983. Breaching the shelfbreak: Passage from youthful to mature phase in submarine canyon evolution. SEPM Special Publication No. 33, pp. 25–39.

Freeze, R.A., Cherry, J.A., 1979. Groundwater. Prentice Hall, Englewood Cliffs, NJ, 604 pp.

Furbish, D.J., 1997. Fluid Physics in Geology. Oxford University Press, New York, 476 pp.

Gibson, R.E., 1958. The progress of consolidation in a clay layer increasing in thickness with time. Géotechnique 8, 171–182.

Harris, C.K., Wiberg, P.L., 2001. A two-dimensional, time-dependent model of suspended sediment transport and bed reworking for continental shelves. Comput. Geosci. 27, 675–690.

Imran, J., Harff, P., Parker, G., 2001. A numerical model of submarine debris flow with graphical user interface. Comput. Geosci. 27, 717–729.

Janbu, N., 1968. Slope stability computations. Soil Mechanics and Foundation Engineering Report, Technical University of Norway, Trondheim.

Julien, P.Y., 1995. Erosion and Sedimentation. Cambridge University Press, Cambridge, 280 pp.

Loseth, T.M., 1999. Submarine Massflow Sedimentation: Computer Modelling and Basin Fill Stratigraphy. Springer Lecture Notes in Earth Science vol. 82, 156 pp.

May, J.A., Warme, J.E., Slater, R.A., 1983. Role of submarine canyons on shelfbreak erosion and sedimentation: modern and ancient examples. SEPM Special Publication 33, 325–33.

Mitchum Jr., R.M., Vail, P.R., Sangree, J.B., 1977. Seismic stratigraphy and global changes of sea level; Part 6, Stratigraphic interpretation of seismic reflection patterns in depositional sequences. In: Payton, C.E. (Ed.), Seismic Stratigraphy; Applications to Hydrocarbon Exploration. Am. Assoc. Pet. Geol. Memoir 26, 117–133.

Morehead, M., Syvitski, J.P., Hutton, E.W.H., 2001. The link between abrupt climate change and basin stratigraphy: A numerical approach. Glob. Planet. Sci. 28, 115–135.

Mulder, T., Savoye, B., Syvitski, J.P.M., 1997. Numerical modelling of the sediment budget for a mid-sized gravity flow: the 1979 Nice turbidity current. Sedimentology 44, 305–326.

O'Grady, D.B., Syvitski, J.P.M., 2001. Predicting profile geometry of continental slopes with a multiprocess sedimentation model. In: Merriam, D.F., Davis, J.C. (Eds.), Geological Modeling and Simulation: Sedimentary Systems. Kluwer Academic/Plenum Publishers, New York, pp. 99–117.

Pratson, L., Imran, J., Hutton, E.W.H., Parker, G., Syvitski, J.P.M., 2001. BANG1D: A one-dimensional, Lagrangian model of subaqueous turbid clouds. Comput. Geosci. 27, 701–716.

Pratson, L., Imran, J., Parker, G., Syvitski, J.P.M., Hutton, E.W.H., 2000. Debris flow versus turbidity currents: A modeling comparison of their dynamics and deposits. In: Bouma, A.H., Stone, C.G. (Eds.), Fine-Grained Turbidite Systems. AAPG Memoir 72 and SEPM Special Publication 68, 57–71.

Ross, W.C., Halliwell, B.A., May, J.A., Watts, D.E., Syvitski, J.P.M., 1994. Slope readjustment: A new model for the development of submarine fans and aprons. Geology 22, 511–514.

Skene, K., Mulder, T., Syvitski, J.P.M., 1997. INFLO1: A model predicting the behaviour of turbidity currents generated at a river mouth. Comput. Geosci. 23, 975–991.

Skene, K., Piper, D.J.W., Aksu, A.E., Syvitski, J.P.M., 1998. Evaluation of the global oxygen isotope curve as a proxy for Quaternary sea level by modeling of delta progradation. J. Sediment. Res. 68, 1077–1092.

Steckler, M.S., 1999. High resolution sequence stratigraphic modeling: 1. The interplay of sedimentation, erosion and subsidence. In: Harbaugh, J., Watney, L., Rankey, G., Slingerland, R., Goldstein, R., Franseen, E. (Eds.), Numerical Experiments in Stratigraphy. SEPM Memoir 62, 139–149.

Syvitski, J.P.M., Alcott, J.M., 1995. DELTA6: Numerical simulation of basin sedimentation affected by slope failure and debris flow runout. In: Pierre Beghin International Workshop on Rapid Gravitational Mass Movements, Grenoble, pp. 305–312.

Syvitski, J.P., Hutton, E.W.H., 2001. 2D SEDFLUX 1.0C: An advanced process-response numerical model for the fill of marine sedimentary basins. Comput. Geosci. 27, 731–754.

Syvitski, J.P.M., Hutton, E.W.H., 2003. Failure of marine deposits and their redistribution by sediment gravity flows. J. Appl. Phys. 160, 2053–2069.

Syvitski, J.P.M., Nicholson, M., Skene, K., Morehead, M.D., 1998. PLUME1.1: Deposition of sediment from a fluvial plume. Comput. Geosci. 24, 159–171.

Warrick, R.A., 1993. Climate and sea level change: A synthesis. In: Warrick, R.A., Barrow, E.M., Wigley, T.M.L. (Eds.), Climate and Sea Level Change: Observations, Projections and Implications. Cambridge University Press, Cambridge, pp. 3–21.

Wilson, R.C., Keefer, D.K., 1983. Dynamic analysis of a slope failure from the 1979 Coyote Lake, California, earthquake. Bull. Seismol. Soc. America 23, 863–877.

Wright, L.D., Friedrichs, C.T., Kim, S.C., Scully, M.E., 2001. Effects of ambient currents and waves on gravity-driven sediment transport on continental shelves. Mar. Geol. 175, 25–45.